Passive Path Imbalance Measurement in Fiber Optic Interferometer using Homodyne PGC Scheme

Shubham Mirg and Pradeep Kumar K.
Department of Electrical Engineering, Indian Institute of Technology Kanpur, Kanpur-208016, India

Keywords: Fiber Optic Interferometer, Homodyne PGC, Path Imbalance Measurement.

Abstract: We demonstrate a passive measurement technique for interferometer path imbalance using homodyne PGC. A 20.8 kHz frequency modulated optical source is employed to interrogate an unbalanced Michelson interferometer. The spectrum of the received photocurrent is then recorded for various frequency deviation values. The variation in harmonic peak powers enables us to determine path imbalances. Different path imbalances are estimated and verified against the pre-calibrated values. The measurement scheme proposed requires no feedback and can be employed to passively measure path imbalances in interferometer sensor arrays already laid out in the field.

1 INTRODUCTION

Fiber interferometeric sensors work by transducting the measurand induced strain into a phase shift in the optical carrier used for interrogation (Udd and Spillman Jr, 2011), (Santos and Farahi, 2014). The phase shift can be converted into intensity changes by inducing a path difference between the arms of the interferometer.

The environmental perturbations from changes in temperature, mechanical vibrations etc. cause a slowly varying phase drift in the interferometer which in turn severely alters the operating point of the interferometer thus hindering the linear recovery of high frequency phase shifts. This problem is called the fading problem (Sheem et al., 1982) and can be circumvented by employing passive interrogation techniques(Cranch et al., 2003). Two of the most widely used techniques for passive interrogation are homodyne phase generated carrier (PGC) (Dandridge et al., 1982) and differential delay heterodyne (Henning, 1983). Both of techniques employ unbalanced interferometers and thus a passive technique to recalibrate the sensors after they have been laid out in the field is also required. Differential Delay Heterodyne uses pulses at a temporal shift equal to the optical path delay. Having a frequency shift between the two pulse enables to have a phase modulated heterodyne carrier output at the photodiode. The sine and cosine components of phase of interest are obtained by synchronously mixing the photocurrent with in-phase and quadrature version of heterodyne frequency. Homodyne PGC scheme involves the frequency modulation of the interrogating optical input and the received signal involves extracting sine and cosine of phase of interest from the harmonics of the received signal by synchronously mixing them with appropriate frequencies. From the sine and cosine of phase of interest approaches like arctangent and Differentiation and Cross multiplication (DCM) are used to recover the signal of interest. Knowledge of path imbalance is important in the above demodulation techniques for appropriate scaling of the sine and cosine terms by varying the frequency deviation suitably.

The path lengths of each arm can be calibrated in lab environment and the difference can be used to measure the path imbalance. However in scenarios where calibration in lab environment is not feasible such as underwater fiber optic hydrophone array (Cranch et al., 2003), a passive path imbalance measurement technique is required. The amplitudes of harmonic peaks in the spectrum of the received photocurrent in homodyne PGC scheme are in proportion to Bessel functions. The arguments of whom are dependent on frequency deviation and imbalance in the interferometer. By using properties of Bessel's J_n recurrence relation (Sudarshanam and Srinivasan, 1989), (Jin et al., 1991) and (Huang and Lin, 2008), argument of Bessel function can be recovered. However this requires reading upto at least four harmonics of the FM frequency, which in some situations be limited by the bandwidth of the photode-

Mirg, S. and K., P.
Passive Path Imbalance Measurement in Fiber Optic Interferometer using Homodyne PGC Scheme.
DOI: 10.5220/0007407500730078
In *Proceedings of the 7th International Conference on Photonics, Optics and Laser Technology (PHOTOPTICS 2019)*, pages 73-78
ISBN: 978-989-758-364-3

tectors employed. By varying frequency deviation over a range of frequencies and fitting with appropriate Bessel functions trace for only first two harmonics, we demonstrate the argument can be obtained and hence the path imbalance can be determined.

In this paper we demonstrate a passive path difference measuring technique by employing homodyne PGC scheme for demodulation in a Michelson interferometer setup with delay coils. By varying frequency deviation over a 1 GHz range we record the data for various path imbalances. Successful determination of path imbalances is shown and various potential applications are discussed.

The rest of the paper is organized as follows. In Section 2 we discuss the principle of operation and mathematical analysis of homodyne PGC technique. The experimental setup is discussed in Section 3 and corresponding results are discussed in Section 4. Finally, we conclude our work by summarizing the results obtained in Section 5.

2 MATHEMATICAL ANALYSIS

The phase shift of an optical signal over a fiber of length L is given by

$$\phi = \frac{2\pi n L v}{c}, \tag{1}$$

where n is the refractive index of the fiber, c is velocity of light in free space and v is the frequency of carrier. Differentiating (1) yields

$$\frac{\Delta\phi}{\phi} = \frac{2\pi}{c}\left(\frac{\Delta L}{L} + \frac{\Delta n}{n} + \frac{\Delta v}{v}\right). \tag{2}$$

From Eq. (2), it can be seen that changes in length(ΔL), refractive index (Δn) and frequency (Δv) can induce a phase change in the optical carrier. The first two changes can be induced by measurand induced strain, hence creating a transduction mechanism. Further the change in frequency can be used to passively interrogate the optical fibers by modulating the input frequency.

2.1 Homodyne PGC

Homodyne PGC scheme involves the interrogation of an unbalanced interferometer with a frequency modulated(FM) optical carrier as the input signal. The schematic is shown in Figure 1. A measurand induced phase change $\phi_a(t)$ is assumed in one arm of the interferometer. The modulated frequency $\omega(t)$ of the FM optical carrier is given by

$$\omega(t) = 2\pi[f_o + \Delta v_o \cos(\omega_{fm} t)] \tag{3}$$

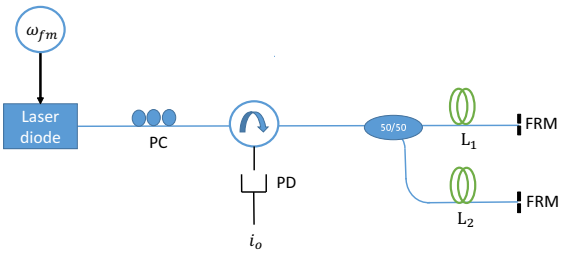

Figure 1: Schematic diagram for homodyne PGC scheme in a Michelson interferometer setup. PC: Polarization controller, PD: Photodiode.

where f_o is the carrier frequency and Δv_o is the maximum frequency deviation. The equation of the electric-field of the FM optical carrier $E(t)$ is given by

$$E(t) = E_o \exp\left[j\left[2\pi f_o t + \frac{2\pi\Delta v_o}{\omega_{fm}}\sin(\omega_{fm} t) + \phi_p(t)\right]\right] + c.c, \tag{4}$$

where E_o is the field amplitude and $\phi_p(t)$ is the phase noise. The net time delay τ in traversing each arm of length difference ($\Delta L = |L_1 - L_2|$) twice in the interferometer is given as

$$\tau = \frac{n 2\Delta L}{c}. \tag{5}$$

The incident electric field at the photodetector input ($E_{out}(t)$) is then given by

$$E_{out}(t) = E_1(t) + E_2(t+\tau). \tag{6}$$

Using Eqs. (3), (4) and (5) the photocurrent output $i_o(t)$ of the interferometer is given by

$$i_o(t) = R\left[P_1 + P_2 + 2V\sqrt{P_1 P_2}\cos(\Delta\phi(t))\right], \tag{7}$$

where R is the responsivity of the photodiode, P_1 and P_2 are the average powers from each arm in the absence of interference, V is the fringe visibility and the phase difference ($\Delta\phi(t) = arg(E(t+\tau)) - arg(E(t))$) between two arms is given by

$$\Delta\phi(t) = 2\pi f_o \tau + \phi_a(t) + \phi_n(t) + \phi_p(t+\tau) - \phi_p(t) + \phi_{fm}(t), \tag{8}$$

where $\phi_a(t)$ is the phase change because of the measurand, $\phi_n(t)$ is the phase change due to environmental perturbations and $\phi_{fm}(t)$ is given by

$$\phi_{fm}(t) = \frac{2\pi\Delta v_o}{\omega_{fm}}[2\cos(\omega_{fm}(t+\tau/2))\sin(\omega_{fm}\tau/2)]. \tag{9}$$

For small τ, Eq. (9) can be approximated as

$$\phi_{fm}(t) \approx \frac{4\pi n \Delta v_o \Delta L}{c}\cos(\omega_{fm} t). \tag{10}$$

The photodetector current can then be written as

$$i_o(t) = R[P_1 + P_2 + P\cos(\mu\cos(\omega_{fm}t) + \phi_o(t))], \quad (11)$$

where P=$V\sqrt{P_1P_2}$, μ=$4\pi n\Delta\nu_o\Delta L/c$ and $\phi_o(t)$=$(2\pi f_o\tau + \phi_a(t) + \phi_n(t) + \phi_p(t+\tau) - \phi_p(t))$. It is noteworthy in Eq. (11), that $\phi_o(t)$ contains measurand information, while μ is in proportion to the path imbalance. Eq. (11) can be expanded using Bessel functions as

$$\begin{aligned} & i_o(t) \\ & = R[P_1 + P_2] + RP\Bigg[\Bigg[J_0(\mu) \\ & \quad + \sum_{n=1}^{n=\infty} J_{2n}(\mu)(-1)^n\cos(2n\omega_{fm}t)\Bigg]\cos(\phi_o(t)) \\ & \quad - \Bigg[\sum_{n=1}^{n=\infty} J_k(\mu)(-1)^n\cos((k)\omega_{fm}t)\Bigg]\sin(\phi_o(t))\Bigg], \end{aligned} \quad (12)$$

where k=2n-1. The next step in the scheme involves extracting the sine and cosine of phase $\phi_o(t)$ by mixing the current with $\cos(\omega_{fm}t)$ and $\cos(2\omega_{fm}t)$ followed by low pass filtering as shown in Figure 2. The two terms are given by

$$i_{o1}(t) = RPJ_1(\mu)\sin(\phi_o(t)), \quad (13)$$

$$i_{o2}(t) = -RPJ_2(\mu)\cos(\phi_o(t)). \quad (14)$$

Methods such as Arctangent and DCM are then employed to extract $\phi_o(t)$. We instead obtain the spectrum of i_o in Eq. (12) directly to find the harmonics peak information, to determine the argument μ and hence the path imbalance in the interferometer.

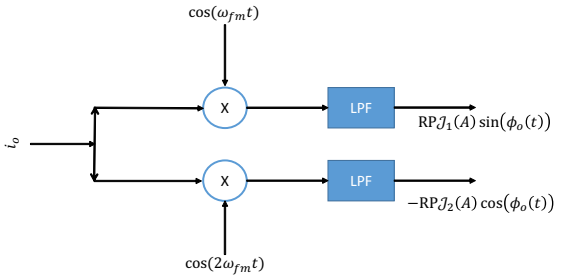

Figure 2: Schematic diagram for obtaining in-phase and quadrature phase of interest.

2.2 Path Imbalance Measurement

Argument of Bessel function (μ) is in direct proportion to frequency deviation, therefore by varying frequency deviation over a certain range the peak values of the FM harmonics in the spectrum changes accordingly. This is demonstrated by numerically plotting the spectrum of $i_o(t)$ in Figure 3, assuming RPV=10 a.u, $\phi_o(t) = \pi/4$, μ=1, frequency modulation=20.8 kHz and sampling frequency in numerical calculation was taken as 180 kHz.

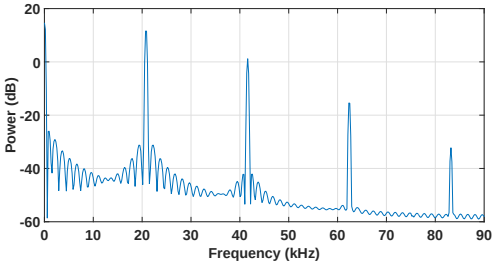

Figure 3: Numerical plot of spectrum of photocurrent $i_o(t)$ given in Eq. (12). F.M=20.8 kHz, μ=1, $\phi_o(t) = \pi/4$ and RPV=10 a.u.

A frequency deviation sweep over a certain range will lead to a change in peaks which follow $J_n^2(\mu)$ characteristics as shown in Figure 4 for $J_1^2(\mu)$ and $J_2^2(\mu)$ where

$$\mu = \beta\Delta\nu_o \quad (15)$$

and ΔL from Eq. (10) and (15) can then be found using the expression

$$\Delta L = \frac{\beta c}{4\pi n}. \quad (16)$$

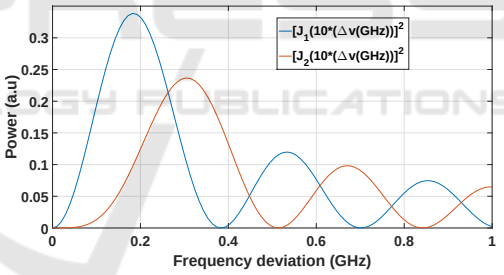

Figure 4: J_1^2 and J_2^2 plotted against frequency deviation with $\beta = 10$ GHz^-1.

3 EXPERIMENTAL SETUP

Figure 5 shows the experimental setup. Keysight N7714A Tunable laser source was employed with 20.8 kHz frequency modulation and frequency deviation control over 0 to 1 GHz in steps of 0.1 GHz. Tunable laser source also induces a 800 Hz dither frequency modulation for frequency stabilization. The effect of this dither frequency is reflected as side bands to the harmonics of 20.8 kHz . This was followed by a polarization controller to control the input polarization of light. The optical carrier was then input to port 1 of the circulator. Port 2 of the circulator is connected to Michelson interferometer with two

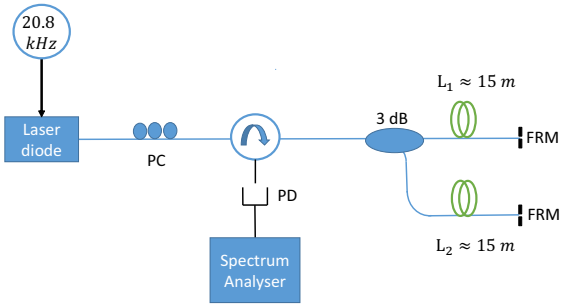

Figure 5: Experimental setup for path imbalance measurement. PC: Polarization controller, PD: Photodiode.

delay coils of around 15 m initial lengths. The coils were followed by Faraday rotating mirrors (FRM) to circumvent polarization fading. At port 3 of the circulator a photodiode converts the input signal to electrical photocurrent which is then analysed using an radio frequency (RF) spectrum analyser. The data is acquired at the entire frequency deviation range of 0 to 1 GHz . The coil is then shortened and the amount of length removed is noted. The readings are taken at 5 different path imbalances. The obtained value of length difference of two consecutive path imbalances is then matched with calibrated length difference.

The variation in spectrum output at frequency deviation 0.1 GHz and 0.8 GHz is shown in Figure 6 and 7. The side bands of 800 Hz are due to the laser source induced dither frequency modulation. The peak power at 20.8 kHz and 41.6 kHz is averaged and stored over the entire frequency deviation range.

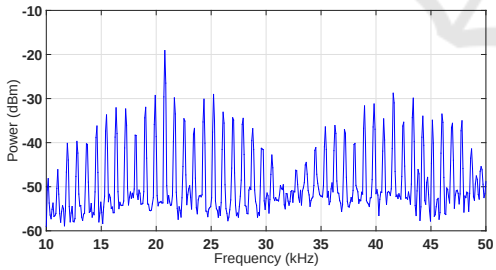

Figure 6: Spectrum analyser output with frequency deviation 0.1 GHz.

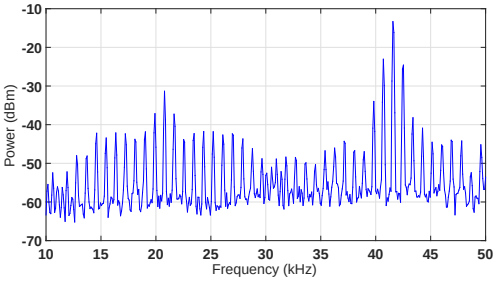

Figure 7: Spectrum analyser output with frequency deviation 0.8 GHz.

4 RESULTS AND DISCUSSIONS

The traces of first (20.8 kHz) and second harmonic (41.6 kHz) peak powers are plotted against frequency deviation upto 1 GHz in steps of 0.1 GHz for five different path imbalances. The traces and curve fit are shown in Figure 8-10 for three different path imbalances in descending order. As the path imbalance is decreased, the curves begin to expand on the x axis, due to the direct proportion dependence of arguments of Bessel function and path imbalance. Traces are then fitted with both harmonics power being in proportion to $J_1(\beta\Delta v_o)^2$ and $J_2(\beta\Delta v_o)^2$.

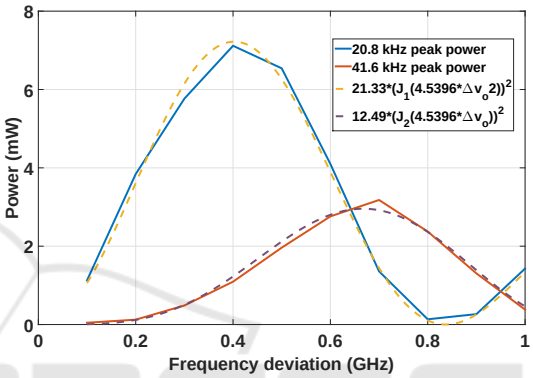

Figure 8: Path imbalance 1: Trace and appropriate curve fittings for first two harmonic peak powers from the spectrum of $i_o(t)$ for the frequency deviation range of 0.1-1 GHz. β is obtained as 4.5396 GHz^{-1}.

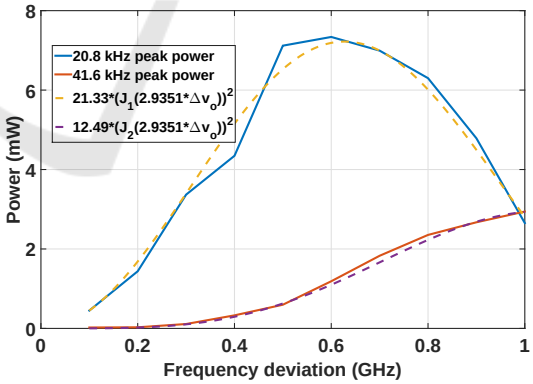

Figure 9: Path imbalance 2: Trace and appropriate curve fittings for first two harmonic peak powers from the spectrum of $i_o(t)$ for the frequency deviation range of 0.1-1 GHz. β obtained as 2.9351 GHz^{-1}.

The different value of β for different path imbalance cases is shown in Table 1 and the estimated path imbalance is calculated using Eq. (16) using n=1.445, c=3 × 10^8 m/s, followed by estimated difference in consecutive path imbalances ($\delta(\Delta L)$) and the last column shows the calibrated length difference ($\delta(\Delta L)$).

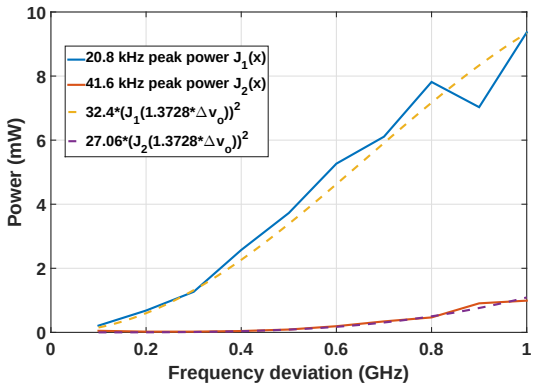

Figure 10: Path imbalance 4: Trace and appropriate curve fittings for first two harmonic peak powers from the spectrum of $i_o(t)$ for the frequency deviation range of 0.1-1 GHz. β obtained as 1.3728 GHz^{-1}.

The two values are mismatched, however as seen in Table 2, the mismatch is a constant scaling factor with a mean value of 0.34. This constant scaling factor can then be employed to correct our path imbalance estimation as seen in Table 3 using the equation

$$\Delta L' = \frac{\Delta L}{0.34}. \tag{17}$$

We believe this scaling factor is inherent to the laser diode's frequency modulation through current modulation, further study is needed to determine the root cause of the scaling factor. A measure of path imbalance without feedback is thus obtained using the above scheme. The scaling factors can be calibrated for the frequency modulated optical source and can directly be implemented in the field passively using just the received photocurrent spectrum in a homodyne PGC setup.

5 CONCLUSIONS

In summary, we have demonstrated a path imbalance measurement technique which can directly be employed in the field using the existing homodyne PGC setup. We began by deriving the mathematical equations needed to predict the behaviour of the output current spectrum in our PGC setup. Experimental estimation of multiple path imbalances were carried out by tracing the first and second harmonic peaks in the spectrum of $i_o(t)$ and then fitting them with appropriate curves on the basis of mathematical analysis, to estimate the argument of the Bessel functions. A scaling factor of 0.34 was obtained from comparing the length difference of two consecutive path imbalances estimated to the calibrated path difference. With the frequency modulated optical source characterized and the scaling factor known, we estimated the different path imbalances. The measurement involves no feedback and can be used in the field environment to estimate path imbalances in the interferometers.

Table 1: Values of β, Scaled path imbalance (ΔL), Estimated length difference between consecutive configurations ($\delta(\Delta L)$) and Calibrated values of length difference ($\delta(\Delta L)_{cal}$).

Case	β (GHz^{-1})	ΔL (cm)	$\delta(\Delta L)$ (cm)	$\delta(\Delta L)_{cal}$ (cm)
1	4.5396	7.5	–	–
2	2.9351	4.85	2.65	7.5
3	2.179	3.6	1.25	3.7
4	1.3728	2.27	1.33	3.9
5	0.7191	1.19	1.08	3.3

Table 2: Ration of estimated length difference to calibrated length difference.

$\delta(\Delta L)$(cm)	$\delta(\Delta L)_{cal}$(cm)	$\frac{\delta(\Delta L)}{\delta(\Delta L)_{cal}}$
2.65	7.5	0.3533
1.25	3.7	0.3378
1.33	3.9	0.3410
1.08	3.3	0.3273

Table 3: Estimated path imbalance after appropriate scaling ($\Delta L'$).

β(GHz^{-1})	$\Delta L'$(cm)
4.5396	22.059
2.9351	14.264
2.179	10.588
1.3728	6.676
0.7191	3.5

REFERENCES

Cranch, G. A., Nash, P. J., and Kirkendall, C. K. (2003). Large-scale remotely interrogated arrays of fiber-optic interferometric sensors for underwater acoustic applications. *IEEE Sensors Journal*, 3(1):19–30.

Dandridge, A., Tveten, A. B., and Giallorenzi, T. G. (1982). Homodyne demodulation scheme for fiber optic sensors using phase generated carrier. *IEEE Transactions on Microwave Theory and Techniques*, 30(10):1635–1641.

Henning, M. (1983). Optical fiber hydrophones with down lead insensitivity. In *Proc. First International Conference on Optical Fiber Sensors, London, 1983*, pages 23–27.

Huang, S.-C. and Lin, H. (2008). Method for path imbalance measurement of the two-arm fiber-optic interferometer. *Appl. Opt.*, 47(28):5065–5073.

Jin, W., Zhang, L. M., Uttamchandani, D., and Culshaw, B. (1991). Modified j1 ... j4 method for linear readout of dynamic phase changes in a fiber-optic homodyne interferometer. *Appl. Opt.*, 30(31):4496–4499.

Santos, J. L. and Farahi, F. (2014). *Handbook of optical sensors*. CRC Press.

Sheem, S. K., Giallorenzi, T. G., and Koo, K. (1982). Optical techniques to solve the signal fading problem in fiber interferometers. *Appl. Opt.*, 21(4):689–693.

Sudarshanam, V. S. and Srinivasan, K. (1989). Linear readout of dynamic phase change in a fiber-optic homodyne interferometer. *Opt. Lett.*, 14(2):140–142.

Udd, E. and Spillman Jr, W. B. (2011). *Fiber optic sensors: an introduction for engineers and scientists*. John Wiley & Sons.